The mobility of phosphorus, iron, and manganese through the sediment–water continuum of a shallow eutrophic freshwater lake under stratified and mixed water-column conditions

Article *in* Biogeochemistry · January 2016

DOI: 10.1007/s10533-015-0144-x

CITATIONS
52

READS
742

6 authors, including:

Courtney Giles
University of Vermont
43 PUBLICATIONS **893** CITATIONS
SEE PROFILE

Peter D.F. Isles
Vermont Department of Environmental Conservation
43 PUBLICATIONS **386** CITATIONS
SEE PROFILE

Tom Manley
Sir Parshurambhau College
54 PUBLICATIONS **1,164** CITATIONS
SEE PROFILE

Yaoyang Xu
University of Vermont
13 PUBLICATIONS **212** CITATIONS
SEE PROFILE

Biogeochemistry
DOI 10.1007/s10533-015-0144-x

The mobility of phosphorus, iron, and manganese through the sediment–water continuum of a shallow eutrophic freshwater lake under stratified and mixed water-column conditions

Courtney D. Giles · Peter D. F. Isles · Tom Manley · Yaoyang Xu · Gregory K. Druschel · Andrew W. Schroth

Received: 13 May 2015 / Accepted: 28 September 2015

Abstract The management of external nutrient inputs to eutrophic systems can be confounded due to a persistent pool of phosphorus (P) in lake sediments. The behaviors of P and trace metals depend largely on the reductive dissolution of amorphous iron (Fe) and manganese (Mn) (oxy)hydroxides in sediments; however, a holistic understanding of these dynamics in relation to the broader ecological and hydrodynamic conditions of the system remains elusive. We used a high-frequency monitoring approach to develop a comprehensive conceptual model of P, Mn, and Fe dynamics across the sediment water continuum of a shallow bay in Lake Champlain (Missisquoi Bay, USA). The greatest release of sediment P, Mn, and Fe occurred under stable hydrodynamic conditions, particularly during the onset of the cyanobacterial bloom and was associated with low available P and the accumulation of soluble Mn and Fe above the sediment–water interface (SWI). During the warmest part of the season, bloom severity and sediment P release was partially regulated by hydrodynamic drivers, which changed on hourly time scales to affect redox conditions at the SWI and bottom water concentrations of soluble P, Mn, and Fe. A geochemically distinct increase in soluble P and Fe concentrations, but not Mn, marked the influence of riverine inputs during a late season storm disturbance. Despite continued depletion of the reactive sediment P and

Responsible Editor: Maren Voss.

Electronic supplementary material The online version of this article (doi:10.1007/s10533-015-0144-x) contains supplementary material, which is available to authorized users.

C. D. Giles
The James Hutton Institute, Invergowrie, Dundee DD2 5BA, Scotland, UK

C. D. Giles (✉) · P. D. F. Isles · T. Manley · Y. Xu · A. W. Schroth
Vermont Experimental Program to Stimulate Competitive Research, University of Vermont, Burlington, VT 05405, USA
e-mail: courtney.giles@hutton.ac.uk

P. D. F. Isles
Rubenstein School of Environment and Natural Resources, University of Vermont, Burlington, VT 05405, USA

T. Manley
Department of Geology, Middlebury College, Middlebury, VT 15753, USA

G. K. Druschel
Department of Chemistry and Chemical Biology, Indiana University – Purdue University Indianapolis, Indianapolis, IN 46202, USA

A. W. Schroth
Department of Geology, University of Vermont, Burlington, VT 05405, USA

Published online: 19 December 2015

metals pool into the bloom period, declining temperatures and a well-mixed water column resulted in bloom senescence and the return of P, Mn, and Fe to surface sediments. The closed cycling of P and metals in Missisquoi Bay poses a significant challenge for the long-term removal of P from this system. Multiple time-scale measures of physical and biogeochemical changes provide a basis for understanding P and trace metals behavior across sediments and the water column, which shape seasonally variable cyanobacterial blooms in shallow eutrophic systems.

Keywords Phosphorus · Redox cycling · Internal loading · Eutrophication · Hydrodynamics

Introduction

External nutrient sources have been the focus of management in eutrophic systems for decades, however numerous studies have reported contributions from internal sources (such as lake sediments) to the concentration of nutrients in overlying waters (Sondergaard et al. 2007). Several studies have identified geochemical mechanisms of sediment phosphorus (P) release in shallow, eutrophic systems associated with redox-driven processes (Andersen and Ring 1999; Ann et al. 2000; Das et al. 2009; Holdren and Armstrong 1980; Moore et al. 1998; Olila and Reddy 1997; Smith et al. 2011; Zilius et al. 2014). The relative contribution of these internal mechanisms to P release may depend on the frequency and duration of mixing events (e.g., wind, precipitation, riverine discharge) and water column stability (Thomas and Schallenberg 2008), as well as feedbacks between biological productivity and water column oxygenation (e.g., benthic oxygen demand via heterotrophic respiration, photosynthetic oxygen production; Zilius et al. 2014). In order to better predict the response of aquatic systems to the increased frequency and severity of climate-related storm disturbance, warming, or changing seasonality, an improved conceptual model of the abiotic and geochemical drivers of internal P loading is needed (Huber et al. 2012; O'Neil et al. 2012). Targeted studies that integrate both biogeochemical and hydrodynamic processes are noticeably absent from the literature, but could greatly improve our understanding of internal loading processes and the associated feedback cycles of P and trace metals that drive the propagation of algal blooms in eutrophic systems.

Periods of prolonged calm can lead to the development of transient thermal stratification, preventing reaeration, and resulting in the depletion of dissolved oxygen in bottom water layers (Coloso et al. 2011; Friedrich et al. 2014). Oxygen depletion associated with heterotrophic respiration largely controls the redox status of the sediment–water interface (SWI) in shallow lakes (Holdren and Armstrong 1980; Hupfer and Lewandowski 2008; Moore et al. 1998). Early geochemical models of P diffusivity in freshwater sediments suggest that the interface between oxidized surface sediments and sub-oxic buried sediments (redox front) will act as a 'trap' for oxidized metals (Froelich et al. 1979). This junction is often characterized by a concentrated layer of Mn- and Fe-oxides near the SWI. Iron-oxides will sequester P via sorption at typical environmental pH (5–8; Katsev and Dittrich 2013); Mn-oxides do not generally sorb significant P, but are typically reduced first (Madison et al. 2013). Manganese and Fe dynamics have been linked to the mobility of sediment P in many eutrophic freshwater and marine systems (Canfield et al. 2005; Hupfer and Lewandowski 2008; Smith et al. 2011, Pearce et al. 2013). These phenomena have been characterized through the use of microelectrodes to record shifts in the location of the sediment redox front over an algal bloom period in a shallow eutrophic bay (Smith et al. 2011). Maxima in the occurrence of reduced Mn^{2+} and Fe^{2+} species and O_2 depletion corresponded to the depletion of reactive P in sediments and peak cyanobacterial concentrations (Smith et al. 2011). In a related study, Pearce et al. (2013) found that anoxia and the presence of reduced Mn^{2+} species in sediments and bottom waters were strong indicators of bloom occurrence, and suggested that the reduction of Mn may precede that of Fe, indicating the release and internal enrichment of algal-available P in shallow eutrophic systems.

Interesting feedbacks between ecological, hydrodynamic, and SWI biogeochemical processes have been documented in shallow systems. The temperature threshold for most bloom-forming cyanobacteria occurs around 25–30 °C, which much be achieved for maximum growth under sufficient nutrient and light conditions (Butterwick et al. 2005). Furthermore, cyanobacterial dominance has been linked to calm and stratified hydrodynamic conditions in shallow systems, which provide a competitive advantage to

cells with the ability to regulate buoyancy and maximize both surface water light and bottom water nutrient resources (Huber et al. 2012; Huisman et al. 2004; Reynolds et al. 1987). At high densities, cyanobacterial blooms cause light limitation, leading to reductions in photosynthetic oxygen production in deeper waters. Under these conditions, ongoing respiration of benthic heterotrophs can lead to oxygen depletion in bottom waters and the establishment of positive feedbacks between bloom productivity and the development of reducing conditions at the SWI (and presumably P and metal loading; Cremona et al. 2014; Torremorell et al. 2009). The interdependence of lake hydrodynamics, ecological productivity, and redox status at the SWI suggest that seasonal and short-term variations in water column stability and temperature could influence the redox-driven release of sediment P and the progression of cyanobacterial blooms over similar time scales.

Although the coupled behavior of P and metals has been demonstrated previously (Deborde et al. 2008; Pearce et al. 2013; Smith et al. 2011), a comprehensive model of their behavior and cycling remains elusive in shallow lake systems. An understanding of these processes could prove critical for predicting the magnitude of internal P loading in response to shifts in climate. The overarching objective of this study is to combine high-frequency water quality, meteorological, and hydrodynamic sensor-based monitoring with time-series sediment and aqueous geochemical measurements to describe the drivers of internal P, Fe and Mn dynamics in shallow eutrophic lakes. We use a comprehensive biological, geochemical and hydrodynamic time-series dataset from the well-characterized, shallow, and eutrophic Missisquoi Bay of Lake Champlain to: (1) identify periods of stable and disturbed water column conditions, (2) determine the distribution of P and metals in the sediment–water continuum on weekly to biweekly time-scales, (3) quantify the depletion and accumulation (flux) of reactive P and metals in the sediments, and (4) develop a holistic conceptual model of P and metals partitioning over the course of a bloom season.

Materials and methods

Study site

Located in the northeastern quadrant of Lake Champlain, Missisquoi Bay is a shallow, eutrophic or pseudoeutrophic ecosystem, which is considered at risk for increased eutrophication due to excessive P (Xu et al. 2015). The watershed is 3105 km^2 (767,246 ac) and the bay surface area is $\sim$77.5 km^2 (19,150 acres), with a maximum depth of approximately 4 m (Hegmen et al. 1999). Fifty-eight percent of the watershed is in Vermont, USA and 42 % in the Province of Quebec, Canada (Troy et al. 2007). Water column concentrations of total P range from 6 to 111 μg L^{-1} and average 49 μg L^{-1} (VTDEC 2008). The bay freezes completely during the winter with ice-cover generally occurring between December and April each year. The study site (N 44°59.503′, W 73°06.798′) is located in the southeast portion of the bay between two river outlets: Missisquoi River to the south and a smaller tributary, Rock River, to the east. Water depth ranges from $\sim$2.9 to 4.0 m over the course of the year. The top 30 cm of sediment are mottled brown-gray, slightly coarser than clay, containing organic-C between 2 and 3 %. Sparse aquatic vegetation, mussels, and invertebrates are found in the area surrounding the study site (Burgess 2007). The sediments become more clay-rich (dark gray and fine-grained) below the recent deposits (60 cm). The recent sedimentation rate is approximately 1 mm $year^{-1}$ (Burgess, 2007).

High-frequency monitoring

Water quality and meteorological data were collected using a modified YSI vertical profiling system attached to an anchored pontoon platform (YSI systems, Yellow Springs MT) and equipped with a YSI 6980 Controller Assembly, a YSI 6955 Winch Assembly, a meteorological (MET) station, and depth sounding unit. The controller assembly housed independent CR1000 dataloggers (Campbell Scientific, Logan UT, USA) for the sonde and MET stations, which were linked to a single modem via PakBus configuration. LoggerNet Pro v.4 software (Campbell Scientific, Logan UT, USA) was used to communicate with the winch and MET dataloggers. Power was supplied to the station by a 12 V battery, interfaced to two solar panels by solar charger/regulator.

The profiler winch assembly was equipped with a YSI 6600V2 sonde containing optical probes, which measured dissolved oxygen (DO, mg L^{-1}) and blue-green algae (BGA) cell density based on phycocyanin (PC) fluorescence (Ratio Fluorescence Units, RFU).

Cyanobacterial biovolume ($mm^3\ L^{-1}$) was previously found to be well-correlated with PC fluorescence in Missisquoi Bay (Zamyadi et al. 2012). Winch movement and sonde parameter collection was programmed to occur hourly at 0.5 m increments throughout the water column. The bottom 1 m of the water column was excluded to prevent collision of the probes with the sediment surface during periods of high wave activity, however manual sonde casts were also conducted during weekly water sampling trips to better characterize bottom water conditions when concurrent samples were collected. We used the difference between surface and bottom water measurements from the winch or manually deployed sondes to indicate the relative stratification of variables over time. Wind speed was measured by an onboard meteorological station (manufacturer info) at 30 min intervals. A wind-mixing threshold of 4.5 m s^{-1} was adopted based on a prior hydrodynamic model of Missisquoi Bay (Isles et al. 2015). The platform was deployed on Julian day (JD) 167 (June 16) and removed for the season on JD 296 (October 27) in 2013. Manual sonde casts (YSI 6600V2) were made on weekly maintenance trips to the profiler platform in order to obtain DO measurements closer to the SWI than the profiler system could safely reach.

Measurement of water column stability

Temperature sensors for the determination of water column stability (E) were suspended from an S2 meteorological buoy, which was positioned approximately 100 m from the biogeochemical sensor platform. The system was equipped with a thermistor string (Richard Brancker Research, Ltd.; RBR) and a single temperature sensor (Campbell Scientific, Inc.) to monitor water column stability. The RBR thermistor string consisted of eight sensors, which were spaced 0.5 m apart beginning at 1.09 m below the surface of the lake. Due to the shallow nature of the bay, only the top five sensors were utilized. To complete the distribution of water column temperature measurements, the solitary CSI sensor was placed at 0.3 m below the lake surface. All temperature observations had manufacturers' stated accuracy of ±0.005 °C. Temperature chain data was collected throughout the study period with the exception of JD 154–163.

Water column stability (E) was calculated based on the relative thermal resistance against mixing (RTRM) method, as described by Coloso et al. (2011):

$$\mathrm{E} = \frac{1}{\rho_0}\frac{\partial \rho}{\partial z} - \frac{g}{c^2} \quad (1)$$

where ρ_0 is the reference density (1 kg L^{-1}), g is the gravitational acceleration (9.80665 m s^{-2}), c is the speed of sound in water (343 m s^{-1}) and density (ρ) was calculated based on the temperature (T) at each depth as follows:

$$\rho = 1 - 6.63 \times 10^{-6}(T-4)^2 \quad (2)$$

Temperature chain measurements were used to calculate hourly stability for each depth interval and to determine the maximum stability in the water column at hourly and daily intervals. Maximum daily stability values were ranked and classified within quartiles for comparison to daily water column data.

Water column sampling

Water column sampling occurred weekly beginning on 16 June and continuing through 23 October. Duplicate water samples were collected in opaque 1L acid-rinsed bottles using a Masterflex peristaltic pump and acid-rinsed tubing (7.5 % hydrochloric acid). The tubing was flushed for approximately 30 s at each depth prior to collection. Water sampling occurred below the air–water interface (surface) and as close to the sediment–water-interface as possible (≤0.5 m, bottom) to a maximum seasonal depth of 4.3 m. Samples for dissolved metals analysis were collected in separate acid-washed polyethylene bottles. All samples were stored on ice and filtered (0.45 µm, polyethersulfone membrane) within 24 h of collection. Filtered samples for soluble reactive P (SRP) measurement and dissolved metals analysis were acidified using trace metal grade 0.1 % hydrochloric acid. Soluble reactive P was determined within 24 h of collection by molybdenum colorimetry with ascorbic acid modification (USEPA 1996) using a Shimadzu 1601 UV–Vis spectrophotometer (10 cm path length; Shimadzu Scientific Instruments Corp., Columbia MD, USA). The lower order of detection for SRP was 0.1 µg L^{-1}. Soluble iron (sFe) and manganese (sMn) concentrations were determined by inductively-coupled-plasma-mass-spectroscopy (ICP-MS, Woods Hole Plasma Facility;

Shiller 2003). Quality assurance and control of trace metal data were monitored with frequent analysis of the composition of Canadian Reference Material SLRS-4 during ICP-MS runs, as well as intermittent analysis of duplicate samples and full process blanks.

Sediment collection

Duplicate sediment cores were collected every 2 weeks using a gravity-coring device fitted with a clear PVC tube (9 cm diam., 20–40 cm length). We chose to collect only the top 1 cm of surface sediments based on previous findings in Missisquoi Bay, which showed that the largest fluctuation in sediment reactive P concentrations due to redox cycling were found in the upper 1 cm of sediments (Smith et al. 2011). Surface sediments (0–1 cm) were collected using an extrusion apparatus and frozen immediately (−20 °C). Sediments were freeze-dried, ground, and homogenized prior to analysis.

Voltammetric analyses

On JD 198, redox conditions at the SWI were monitored using glass Au-amalgam voltammetric electrodes and a manual micromanipulator to profile O_2, Mn^{2+}, Fe^{2+}, and Fe^{3+} at 1 mm intervals above (+50 mm) and below (−20 mm) the SWI of an intact gravity core (Brendel and Luther 1995; Smith et al. 2011). A three electrode system consisting of a silver/silver chloride reference electrode, a platinum counter electrode, and a glass Au-amalgam working electrode with a 500–800 μm diameter tip was used in voltammetric analyses (Brendel and Luther 1995). Cyclic voltammetry was performed between −0.1 and −1.8 V (vs Ag/AgCl) at a scan rate of 1000 mV s^{-1} with a 2 s conditioning step. Voltammetric analyses were carried out with an Analytical Instrument Systems, Inc. DLK-70 potentiostat and computer controller. Analyses were carried out in sets of 10 sequential scans at each sampling interval, with the first three scans discarded (allowing the electrode response to stabilize). Standard additions of manganese were utilized in a surface water sample and concentrations of O_2, Fe^{2+} were quantified after the pilot ion method (Slowey and Marvin-DiPasquale 2012). The concentrations determined by voltammetric analyses were used to calculate the instantaneous flux rate (r, mg m^{-2} d^{-1}) of Mn^{2+} and Fe^{2+} species (i) as follows:

$$r_i = \frac{\partial C_i}{\partial z} \cdot D_i \quad (3)$$

where C_i is the concentration at depth z and D_i is the diffusivity of species i in water, corresponding to 6.88×10^{-6} cm^2 s^{-1} for Mn^{2+} and 7.19×10^{-6} cm^2 s^{-1} for Fe^{2+} (Buffle et al. 2007).

Analysis of sediment geochemistry

Total P and metals were determined by *aqua regia* digestion (EPA method 3050B; USEPA 1996). Briefly, 0.25–0.50 g of dry sediment was extracted with 3:1 HCl:HNO_3 with refluxing for at least 1 h at 80–90 °C. Digestion supernatants were diluted 10-fold and analyzed for P and metals by ICP-OES. Sediments were extracted with ascorbate-citrate-bicarbonate solution (pH 8) to capture the 'reactive' or redox-active fraction of sediment P and metals as described previously (Anschutz et al. 1998; Smith et al. 2011). At alkaline pH, ascorbate-citrate acts as an electron donor to induce the reductive dissolution of amorphous metal phases and the P bound therein. The extractant solution was prepared by dissolving 4 g each of sodium bicarbonate and sodium citrate in 200 mL of deaerated distilled water and slowly adding 10 g L^{-1} ascorbic acid (pH 8). Sediments (0.1–0.2 g dry wt.) were extracted with 1.2 mL ascorbate-citrate-bicarbonate solution for 24 h on an orbital shaker (350 rpm) and centrifuged (6000×g, 5 min) for the collection of supernatants. Extracts were diluted 10-fold prior to analysis of P, Fe, and Mn by ICP-OES.

Calculation of sediment phosphorus and metals flux

Ascorbate-citrate-bicarbonate-extractable concentrations were measured over time to estimate the relative flux of redox-sensitive or 'reactive' P and metals from sediments (Smith et al. 2011; Anschutz et al. 1998). As previously described by Smith et al. (2011), the flux of 'reactive' P and metals is determined based on the difference in sediment extractable concentrations relative to an initial time-point concentration. In this study, the cumulative flux (F_i, mg m^{-2}) was calculated as follows, assuming a sediment bulk density (ρ_s) of 2.5 g cm^{-3} and diffusive thickness (z) of 1 mm:

$$F_i = \left(C_i^{t_0} - C_i^{t_j}\right) \cdot \rho_s \cdot z \quad (4)$$

where C is the concentration of species i (P, Fe, or Mn) and j is a specific time-point (t_j) relative to the reference period (t_0 = 29 January 2013; JD 29). The rate of flux (R, μg L^{-1} d^{-1} or mg m^{-2} d^{-1}) for species i at time j was calculated as follows:

$$R_i^{t_j} = \frac{F_i}{d} \quad (5)$$

where F_i is calculated based on consecutive concentration (C_i) measurements at sampling times $j - 1$ and j, and normalized by the number of days (d) between consecutive sampling dates. When expressed in units of μg L^{-1} d^{-1}, positive R-values represent flux from sediment to water. In units of mg m^{-2} d^{-1}, positive R-values represent the accumulation of P, Fe, or Mn into sediments.

Statistical analyses

Data were analyzed using JMP Pro 10.0.0 (SAS Institute, 2012). Averages and standard errors of P and metals concentrations are based on two to four analytical replicate measures of duplicate aqueous or sediment samples ($4 \leq n \leq 8$) collected in this study. For manual sensor deployments, triplicate measurements are averaged at each depth. Time-series water column and meteorological data from automated sensors represent 30 s averages of each parameter measured hourly during the study period. Bloom period averages are based on composite daily values for each period. All linear correlations between P fractions and sediment depth were evaluated at the $\alpha = 0.05$ significance level.

Results

Definition of bloom periods

The 2013 study period in Missisquoi Bay will be described in terms of discrete algal bloom periods: Pre-bloom (JD 148–187), bloom onset (JD 187–199), bloom (JD 199–246), bloom collapse (JD 246–269), and the late-season bloom (JD 269–296). Bloom periods were primarily defined based on BGA concentrations and water temperature, with secondary support of the physical and abiotic water column data presented in Fig. 1 and described in detail below.

Pre-bloom

The lowest BGA concentrations of the season occurred during the pre-bloom period (Fig. 1a). Water temperatures ranged from 10 to 15 °C at the beginning of the study and increased steadily to ~25 °C by the end of the pre-bloom period (Fig. 1b). The pre-bloom period was marked by the greatest and most prolonged thermal stratification (Fig. 1b) leading to high water column stability (Fig. 1c). This period coincided with the onset of water temperatures suitable for BGA growth (~24 °C; Konopka and Brock 1978). Fifty-eight percent of days in the pre-bloom period were characterized by water column stability in the upper quartile of values for the season ($E > 0.47$ m^{-1}; Fig. 1c). Stable periods lasted from 1 to 6 days during the pre-bloom period and were punctuated by no longer than 3 days of low stability. Maximum stability for the pre-bloom period (1.81 m^{-1}; Fig. 1c) occurred at the end of a stable period and lasted for eight days (JD 169–176). Maximum daily wind speeds in the pre-bloom period were intermediate among bloom period averages for the season and were negatively correlated with water column stability ($r = -0.3247$, $p < .0001$; Fig. 1e).

Generally, data from the continuously deployed sonde did not indicate a strong tendency toward DO stratification during the pre-bloom period, with both surface and bottom water concentrations ranging from 8 to 12 mg L^{-1} and averaging 10 ± 1 mg L^{-1}. One exception to the lack of observed stratification was found in the manual sonde measurements of DO following an extended period of calm (Fig. 2e). Despite the limited DO stratification during the pre-bloom period, there was still a small, albeit significant, correlation between hourly DO stratification and water column stability (Fig. 4; $r = 0.1496$; $p < .0001$). Due to the systematic constraints of the YSI profiler system, weekly manual DO measurements could be made closer to the SWI and would explain the more pronounced stratification of DO in this data set (Figs. 1d, 2e). The difference observed here indicates a strong redox gradient near the SWI on this sampling trip that was not detectable in the depths measured by the winch-sonde system on our monitoring platform.

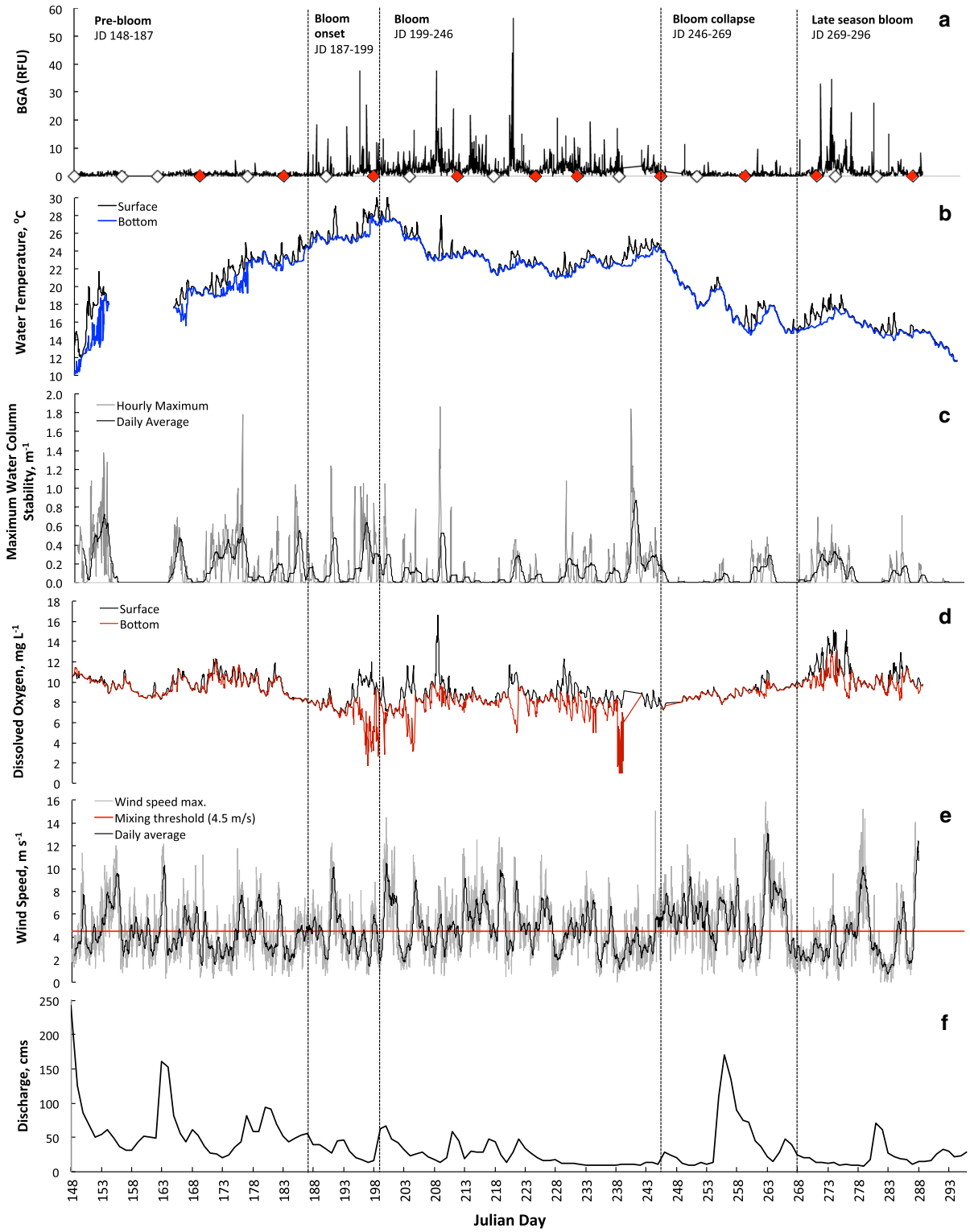
Pre-bloom
JD 148-187
Bloom onset
JD 187-199
Bloom
JD 199-246
Bloom collapse
JD 246-269
Late season bloom
JD 269-296
a
BGA (RFU)
b
Water Temperature, °C
Surface
Bottom
c
Maximum Water Column Stability, m-1
Hourly Maximum
Daily Average
d
Dissolved Oxygen, mg L-1
Surface
Bottom
e
Wind Speed, m s-1
Wind speed max.
Mixing threshold (4.5 m/s)
Daily average
f
Discharge, cms
Julian Day

◀**Fig. 1** Blue green algae (BGA-phycocyanin fluorescence; **a**), water column temperature (**b**), water column stability (**c**), dissolved oxygen concentrations (**d**), hourly maximum and daily average wind speed (**e**), and Missisquoi River discharge (**f**) in 2013 (Julian day 148-296). *Vertical lines* indicate the end of a bloom period. *Diamonds* in (**a**) denote surface water and sediment (*red*) sampling dates. *Horizontal line* in (**e**) represents the previously determined wind-mixing threshold for Missisquoi Bay. (Color figure online)

Both SRP and sFe concentrations were highest on the first sampling date immediately following the largest Missisquoi River discharge event of the spring (Fig. 2d; Online Appendix 1). The concentrations of SRP were relatively low and exhibited little depth stratification for the remainder of the pre-bloom period (Fig. 2a). Total P concentrations ranged from 16 to 60 μg L^{-1} during the pre-bloom period and decreased by 54 % by the end of the period (Fig. 2). SRP represented 41 % of the TP concentration at the beginning of the pre-bloom and diminished to less than 1 % of TP prior to the bloom onset (Fig. 2a, d). Soluble Fe (sFe) concentrations were initially high in surface samples at the beginning of this stage and decreased, whereas sFe remained enriched in bottom waters after the first sampling date (Fig. 2b). Soluble manganese (sMn) concentrations were low at both depths for most of the pre-bloom (<30 μg L^{-1}), with the exception of the bottom water concentration on JD 177, which reached 374.8 μg L^{-1} and occurred 2 days

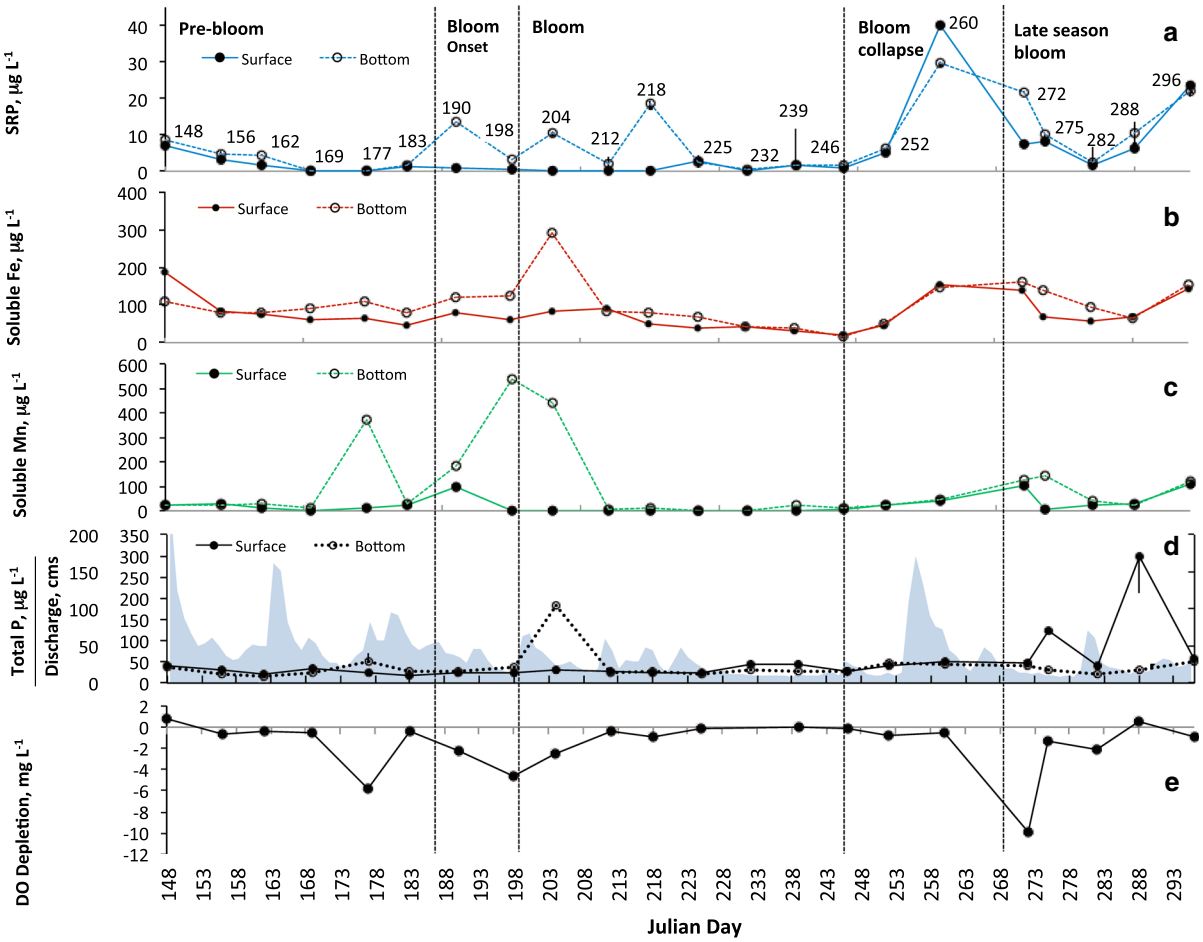

Fig. 2 Soluble reactive phosphorus (SRP, **a**), soluble iron (Fe, **b**), soluble manganese (Mn, **c**), Total P (**d**), and dissolved oxygen depletion (DO, **e**) in surface and bottom waters in Missisquoi Bay. The solid blue series in **d** represents Missisquoi River discharge. Solid and dashed lines (**a**–**d**) represent surface and bottom depths, respectively. DO depletion is defined as the difference between bottom and surface water concentrations. Vertical dashed lines delineate bloom periods. (Color figure online)

after a prolonged period of stability (Figs. 1c, 2c). Low concentrations of sMn (13 μg L^{-1}) and sFe (63 μg L^{-1}) in surface waters led to a substantial differential from the bottom water on this sampling date, which coincided with strong DO depletion at depth (−5.8 mg L^{-1}; Fig. 2b, c, e).

The concentrations of reactive P and metals in surface sediments declined slightly from the first collection date (JD 29) to the pre-bloom (Online Appendix 2). The cumulative flux of reactive P (−1031 mg m^{-2}) was well correlated with that of Mn (−3653 mg m^{-2}; $R^2 = 0.57$) and Fe (−15,451 mg m^{-2}; $R^2 = 0.89$), confirming the coupling of P, Fe, and Mn behavior at the SWI during this phase (Fig. 3). The daily flux rates to the water column calculated from our sediment time series of P (18 μg L^{-1} d^{-1}), Mn (43 μg L^{-1} d^{-1}), and Fe (256 μg L^{-1} d^{-1}) were within an order of magnitude of the concentrations measured in bottom water samples at the end of the pre-bloom (Fig. 2; Online Appendix 2). Soluble reactive P and sMn accumulated in bottom waters, where concentrations were 11.2-fold and 1.4-fold greater than the estimated daily sediment flux rates, respectively. In contrast, the daily flux of Fe from sediments was 3.2-fold greater than what was measured in the bottom water (81 μg L^{-1}; Fig. 2; Online Appendix 2) indicating the partitioning of Fe into other mineral and biological phases or removal via advective processes.

Bloom onset

The bloom onset period (JD 187–199) was characterized by a dramatic increase in phycocyanin fluorescence (BGA) over 2 days, which remained consistently high relative to the pre-bloom period (Fig. 1a). This coincided with the highest water temperatures, the most prolonged and highest water column stability, and the largest DO stratification of the entire study period (Fig. 1). Water column stability was significantly positively correlated with BGA ($r = 0.2019$, $p = .0006$) and DO stratification ($r = 0.4312$, $p < .0001$) and negatively correlated with wind speed ($r = -0.3247$, $p < .0001$) during the bloom onset (Figs. 1, 4). Maxima in BGA occurred during a prolonged period of high surface temperatures (25–31 °C) and thermal stratification, as indicated by consistently high stability values for six

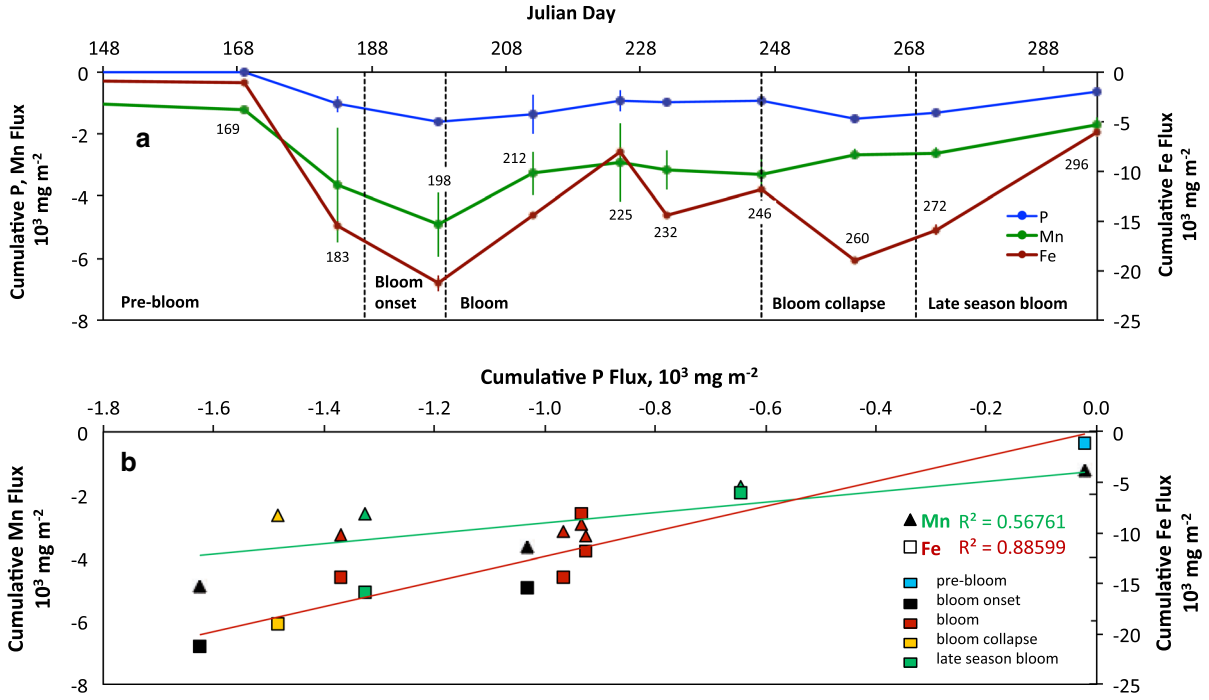

Fig. 3 The cumulative reactive P and metals flux in Missisquoi bay sediments (**a**) and correlations between average sediment reactive P and Mn or Fe sediment fluxes (**b**). Panel A: Numbers correspond to sediment collection days; Negative line slopes between collection days represent depletion, whereas positive line slopes represent the accumulation of P and metals in sediments; Error bars represent standard error of the mean (n = 4). Vertical dashed lines delineate bloom periods. (Color figure online)

consecutive days (Fig. 1a–c). Concurrent with the prolonged period of stability at the end of the bloom-onset, DO stratification persisted over the same 6 days (Fig. 1d). Maximum DO stratification occurred after 4 days of high water column stability and the warmest recorded surface water temperatures (~30 °C; Fig. 1b, c). Average riverine discharge declined to a minimum (Fig. 1f) and wind speed was consistently below the threshold for mixing (4.5 m s^{-1}; Fig. 1e). The greatest stratification of DO corresponded to a prolonged period of water column stability and the warmest recorded surface water temperatures (~30 °C; Fig. 1b, c).

At the beginning of the bloom onset period, SRP, sMn, and sFe exhibited strong bottom water enrichment, which was particularly pronounced in the case of sMn (Fig. 2c). On the second sampling day of the bloom onset period, the stratification of sMn and sFe had increased, while SRP had decreased (Fig. 3). Soluble reactive P represented 2–4 % of the TP concentrations in surface water (~25 µg L^{-1}) and 8–46 % of the TP in bottom water (28–36 µg L^{-1}; Fig. 2). Diminished stratification of bottom and surface concentrations of SRP from JD 190–199 appeared to be due to the depletion of SRP in bottom waters, whereas the sMn differential increased due to both surface water depletion and bottom water enrichment (Fig. 2a, c). As for the pre-bloom period, the spike in sMn concentrations on JD 198 (541 µg L^{-1}) was preceded by a period of stability and associated with a proportionally large depletion of DO with depth (Figs. 1d, 2c, e).

Reactive P and metals concentrations in the sediment reached season minima at the end of the bloom onset period (Online Appendix 2), and corresponded to the maximum cumulative seasonal flux of Fe, Mn, and P from the sediments over the study period (Fig. 3a). Daily flux rates of P (10 µg L^{-1} d^{-1}), Mn (21 µg L^{-1} d^{-1}), and Fe (97 µg L^{-1} d^{-1}) slowed during the bloom onset. SRP concentrations in bottom water were 3-fold less than estimated daily flux values, whereas sFe and sMn concentrations were greater by 1.3-fold and 26-fold, respectively (Figs. 2, 3; Appendix 2). This indicates an outward flux of P and metals, accumulation of sFe and sMn in bottom waters, and the active removal or redistribution of SRP as may be expected from the rapid biological uptake of available P by the developing algal bloom.

The concentration profile of dissolved O_2, Fe^{2+} and Mn^{2+} within the upper 20 mm of the sediment profile confirms that surface sediments were sufficiently reducing to mobilize and maintain reduced forms of these transition metals in solution (Fig. 5). The instantaneous flux rate (r) of Mn^{2+} (−627 mg m^{-2} d^{-1}) in

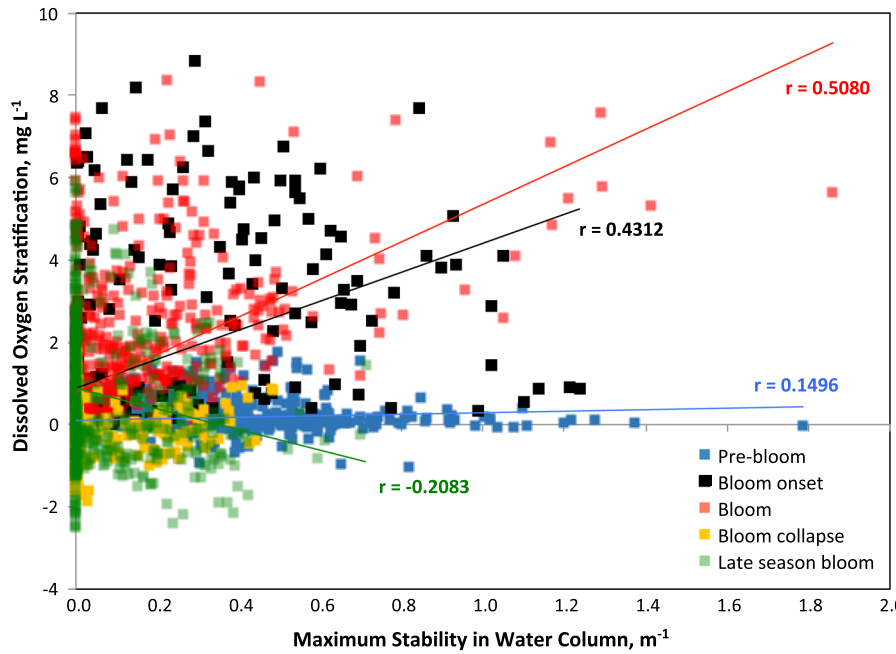

Fig. 4 Hourly maxima in water column stability in relation to hourly dissolved oxygen stratification in the water column of Missisquoi Bay (JD 148–296, 2013). Significant correlation values are indicated in *colored text* corresponding to the bloom periods; For the full study period: r = 0.2149 ($p < .0001$); No significant relationship was found for the bloom collapse period. (Color figure online)

the upper 1 mm of sediments determined by voltammetry was within an order of magnitude of the flux rates (R) determined in the extract-based approach for the same period (JD 198: 84 mg m^{-2} d^{-1}). However, the maximum rate of Mn^{2+} flux occurred at 2 mm below the SWI (−1003 mg m^{-2} d^{-1}). The Fe^{2+} flux rate was greatest at 5 mm below the SWI (−5.29 mg m^{-2} d^{-1}) and was considerably smaller than that determined by ascorbate-citrate-bicarbonate extraction (−388 mg m^{-2} d^{-1}; Online Appendix 2). We speculate that large extract-based estimates of Fe flux are likely an artifact of the selective extraction procedure, which may target a larger pool of Fe mineral phases than those sensitive to reductive dissolution under ambient sediment redox conditions. The voltammetric profile illustrates the small scale stratification of the redoxocline across the SWI as the bloom developed, which was previously inferred due to differences in the manual and automated DO sonde profiles.

Bloom

The bloom period (JD 199–246) was initially characterized by intermittent periods of relatively high BGA cell densities (Fig. 1a) similar to those observed in the bloom onset period. Unlike the prolonged high cell densities reported in previous summers, baseline phycocyanin concentrations during the 2013 bloom were modest in comparison to the bloom onset (e.g., 2012; Isles et al. 2015; http://www.watershedmanagement.vt.gov/lakes/docs/lcmonitoring/lp_lc-phytobiovolumecomp.pdf#zoom=100). Due to a relatively cool summer, average surface water temperatures were lower in the 2013 bloom period (23.7 ± 1.6 °C) compared to bloom onset (26.6 ± 1.3 °C), but remained within a suitable range to support the growth of cyanobacteria (Fig. 1b; Lurling et al. 2013). On average, water column stability diminished in the bloom period due to frequent weather disturbance, as is indicated by the negative correlation with wind speed ($r = -0.3081$; $p < .0001$; Fig. 1c, e; Online Appendix 1). Phycocyanin concentrations persisted through repeated short-lived disturbances (<2 days), which were characterized by low values of water column stability within the lower three quartiles of the season ($E < 0.22$ m^{-1}; Fig. 1c).

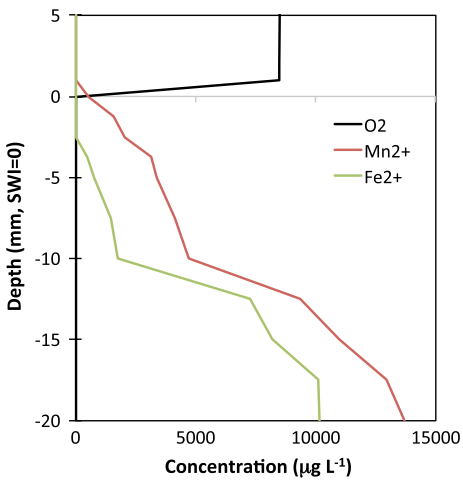

Fig. 5 Concentrations of O_2, Fe^{2+}, and Mn^{2+} species determined by voltammetry from 5 mm above to 20 mm below the sediment water interface (SWI = 0) of an intact sediment core collected from Missisquoi Bay on JD 198. (Color figure online)

Overall, DO stratification was more pronounced in the latter half of the bloom period, particularly on the most stable days. For example, consecutive days of hypoxic conditions were measured in the bottom water (DO < 2 ppm; Friedrich et al. 2014) following a prolonged period of negligible riverine inputs and an intermittent decline of the BGA bloom (Fig. 1a, e; Online Appendix 1). Stratification values for DO ranged from ~6.5 to 7.5 ppm, with bottom water concentrations of 0.5–1.5 ppm. This is also illustrated by the large coefficient of variation between hourly DO stratification and maximum water column stability during the bloom in comparison to other periods ($r = 0.5080$, $p < .0001$; Fig. 4).

Soluble P and metals were highly stratified at the beginning of the bloom period following a period of DO depletion in bottom waters at the end of the bloom onset (Fig. 2d). Soluble Mn and SRP concentrations remained low and unstratified during all additional sampling events during the bloom period (<1–14 µg L^{-1}; Fig. 2a, c). Minimal DO stratification was observed, although it should be noted that intermittent stratification of DO during this stage was evident in the continuously deployed sonde data (Fig. 2c). The lack of stratification of SRP, sMn, and DO concentrations over the course of the bloom corresponded with relatively high average daily wind speeds in excess of 4.5 m s^{-1} and a series of small storms leading to increased discharge from the nearby Missisquoi River (JD 212–221; Fig. 1f). Soluble reactive P (2–2.6 µg L^{-1}) and Fe concentrations (69–84 µg L^{-1}) were greatest in bottom waters during the

bloom period possibly due to the entry of cold, nutrient-rich and oxygenated river waters during this intermittent disturbance period.

Sediment reactive P and metals concentrations increased over the course of the bloom period, as illustrated by smaller negative cumulative flux values and smaller daily flux rates. From JD 212–246, cumulative P and Fe flux decreased by 33 and 18 %, respectively (Fig. 3a). With the exception of JD 232, daily flux rates indicate the accumulation of P (2–34 mg m^{-2} d^{-1}) and Fe (185–491 mg m^{-2} d^{-1}; Fig. 3; Appendix 2). The rate of daily Mn flux was positive only for JD 212 (116 mg m^{-2} d^{-1}) and JD 225 (27 mg m^{-2} d^{-1}), after which depletion persisted until the bloom collapse (Fig. 3; Online Appendix 2). By the end of the bloom period, bottom water concentrations of sMn were 5.5 fold greater than the estimated losses from sediments and 2.5-fold larger than was measured at the beginning of the period (Fig. 2; Appendix 2).

Bloom collapse

The bloom collapse was identified based on a dramatic decrease in phycocyanin beginning in early September, which remained low until the subsequent late season bloom in October. The bloom collapse was initiated by a rapid decline of surface water temperatures (24–14 °C), which was well below the optimal range of cyanobacteria growth (Fig. 1b; Table 1). There were consecutive days of elevated wind speeds, frequent and large storms associated with increased riverine discharge, and diminished water column stability (Fig. 1; Table 1). The relationship between DO stratification and water column stability was not significant during this period ($p = 0.1243$; Fig. 4). However, the coefficient of variation between wind speed and water column stability was the largest and most negative in the bloom collapse ($r = -0.4465$; $p < .0001$) compared to other bloom periods (Fig. 1).

Water column P and metals concentrations were low and non-stratified at the beginning of the bloom collapse, but increased to period maxima following the storm-driven disturbance on JD 260 (Fig. 2). Total P, SRP, and sFe concentrations were among the largest of the study period, particularly in the surface water (Fig. 2a, b, d). As a proportion of total P, SRP increase by more than 10-fold after the storm event and was the largest %SRP measured during the season. On JD 260, SRP represented 66–80 % of the total P in bottom (45 μg TP L^{-1}) and surface (50 μg L^{-1}) waters, respectively (Fig. 2a, d). Soluble Mn concentrations gradually increased in both surface and bottom waters during the bloom collapse (Fig. 2c). The elevated sMn concentrations that proceeded the large discharge event and BGA collapse on JD 260 occurred during a short and rapid period of warming (Fig. 1b), water column stability (Fig. 1c), and DO stratification (Fig. 1d), which persisted despite multiple days of wind speeds greater than 4.5 m s^{-1} (Fig. 1e).

Trends in the flux of sediment P and metals diverged during the bloom collapse period. The cumulative flux of reactive P and Fe increased by 1.6-fold from the end of the bloom to JD 260 (Fig. 3a). The daily flux rates of reactive P (10 μg L^{-1} d^{-1}) and Fe (130 μg L^{-1} d^{-1}) accounted for 34 % and 88 % of the respective SRP and sFe concentrations measured in the bottom water (Fig. 2a, b; Online Appendix 2). In contrast, Mn flux diminished by 20 % over the same time period despite the gradual increase in sMn concentrations during the bloom collapse (Fig. 2c; Online Appendix 2). Estimates of Mn flux indicate that 11.5 μg L^{-1} d^{-1} or 25 % of bottom water sMn concentrations were returning to sediments during the bloom collapse and that alternative sources (e.g., senescing cells) likely contributed to the rising concentrations of sMn measured in the water column (Fig. 2c; Online Appendix 2).

Late season bloom

The physical and biological conditions in Missisquoi Bay changed again as the system transitioned to the late bloom stage. During this transition, there was a decrease in wind speed, minimal discharge from the Missisquoi River, and increasing water temperatures (Fig. 1b, e, f). Increasing water column stability at the beginning of the late bloom was positively correlated with BGA ($r = 0.2453$; $p < .0001$) and DO stratification ($r = 0.2066$; $p < .0001$) and negatively correlated with wind speed ($r = -0.3065$, $p < .0001$; Fig. 1). The average concentration of phycocyanin measured during the late season bloom increased relative to the bloom collapse period to a level that was comparable to the bloom onset stage (Fig. 1a; Table 1). DO stratification developed in both the

Table 1 Biogeochemical and hydrodynamic characteristics of Missisquoi Bay during bloom periods in 2013 based on high-frequency monitoring data

Period	Julian day	BGA	Temperature	Dissolved oxygen mg L^{-1}		Stability	Wind speed	Discharge
		RFU	°C	Surface	Bottom	m^{-1}	m s^{-1}	cms
Full	148–296	1.74 ± 3.01	20.8 ± 4.0	9.4 ± 1.3	8.8 ± 1.4	0.30 ± 0.39	4.3 ± 1.2	38.2 ± 34.5
Pre-bloom	148–187	0.55 ± 0.58	20.8 ± 3.0	9.8 ± 0.9	9.7 ± 0.9	0.51 ± 0.41	4.4 ± 2.2	64.2 ± 42.3
Bloom onset	187–199	1.86 ± 3.49	26.6 ± 1.3	8.5 ± 1.2	7.0 ± 1.4	0.53 ± 0.42	2.7 ± 1.0	32.8 ± 14.9
Bloom	199–246	3.09 ± 3.81	23.7 ± 1.6	8.8 ± 1.0	7.7 ± 1.3	0.31 ± 0.42	4.7 ± 2.4	24.2 ± 15.5
Bloom collapse	246–269	0.66 ± 0.95	18.4 ± 2.4	9.0 ± 0.7	8.9 ± 0.5	0.06 ± 0.16	5.8 ± 2.6	46.0 ± 43.7
Late bloom	269–296	2.11 ± 3.51	15.5 ± 1.5	10.9 ± 1.3	10.1 ± 0.8	0.13 ± 0.23	3.7 ± 2.5	21.4 ± 14.4

Full season and bloom period averages (±SD) correspond to 2013 hourly monitoring data for: blue green algae (BGA) phycocyanin concentrations (ratio fluorescent units, RFU); surface water temperature; maximum water column stability; maximum daily wind speed; Missisquoi River discharge (cubic meters per second, cms) at Swanton, VT

weekly and hourly datasets during this period (Fig. 1d, e).

The second half of the late season bloom period was characterized by a more disturbed water column and a general decline in cyanobacterial populations. Water temperatures declined steadily after this period of stability, with the exception of a two-day period of surface warming, which coincided with a second short increase in BGA growth (Fig. 1a, b). DO stratification and water column stability appeared to be particularly sensitive to prolonged periods of high wind speeds. For example, the end of the stable period from JD 269–277 coincided with wind speed values >4.5 m s^{-1}, whereas the subsequent short (<2 days), stable period occurred as wind speeds fell below this threshold (Fig. 1d, e). The late season bloom was the only study period to result in a negative relationship between DO stratification and stability ($r = -0.2083$, $p < .0001$; Fig. 4).

Water column P and metals concentrations were the most stratified following several days of high stability at the beginning of the late bloom period (Fig. 2). Surface water concentrations of total P increased and were similar to pre-season under-ice concentrations in the late bloom (56–49 μg L^{-1}; Fig. 2d). SRP represented 15–53 % of total P in the water column during the first half of the late bloom period, with the largest proportions occurring in bottom waters (42–53 %; Fig. 2a). The peak in sMn and sFe concentrations occurred 1 week after a substantial period of DO depletion and was not coupled with a measurable increase in SRP concentrations (Fig. 2). Soluble reactive P and metals concentrations began to decline in the middle of the late bloom period, coincident with wind speeds greater than 4.5 m s^{-1} and water column stability in the lower two quartiles of values for the entire season ($E < 0.22$ m^{-1}; Figs. 1, 2). In the absence of significant river inputs during the late season bloom, the large increase in TP on JD 288 may indicate the rapid uptake of mobilized P into algal cells in the first half of the period and the return of P, Mn and Fe to sediments thereafter.

Our sediment time series indicates an extensive accumulation of P, Mn, or Fe during the late season bloom period (Fig. 3a). The first core was collected during the highly stable period in the first half of the late bloom (JD 272) and the final sediment core was collected following a series of storms, wind disturbance, significant decreases in water temperatures and biological activity in the second half (JD 296; Figs. 1, 3a). The rate of sediment reactive P accumulation doubled from −3.3 μg L^{-1} d^{-1} to −7.1 μg L^{-1} d^{-1} during the late season bloom and accounted for the removal of 30–44 % of bottom water SRP concentrations at the end of the study period. Relative to the beginning of the pre-bloom period (JD 169), sediment reactive P, Fe, and Mn concentrations at the end of the late bloom (JD 296) were reduced by 22, 13, 10 %, respectively (Online Appendix 2).

Discussion

Conceptual model: The role of water column stability in redox-driven cycling of P and metals in shallow eutrophic lake systems

Hydrodynamic variability, in this study quantified and monitored as water column stability, was hypothesized to exert a strong influence on P and trace metal dynamics over the course of a bloom season in this shallow, eutrophic system. In order to develop an empirically based conceptual model for Missisquoi Bay, we collected biogeochemical and physical data at multiple time-scales, including hourly water column sensor data (e.g., DO, temperature, BGA), weekly aqueous chemical analysis at two depths, and sediment geochemical data biweekly. The hourly data set provided a robust basis for identifying physical and biological drivers of P and trace metals cycling, whereas weekly measurements of SRP, sMn, and sFe could be used to link these external and internal drivers with biweekly estimates of P and metals partitioning from sediments to the water column. The geochemical assessment revealed the seasonal progression of P release and reaccumulation in sediments, which could be confirmed through concurrent analysis of vertically resolved aqueous chemical and sensor data within the water column.

Discrepancies between sediment flux rates and water column P, Fe, and Mn concentrations require a nuanced interpretation due to the different time-scales of these measurements, as well as the lack of available information on instantaneous rates of P and trace metal transfer between sediment, aqueous, and biotic compartments. However, in the current study, hourly data sets revealed multiple short-lived periods of high water column stability, DO stratification, or rapid warming (<24 h), which manifest as increased bottom water P and metals concentrations and/or transfer to or from sediments on a weekly basis. Additionally, hourly measurements of BGA population dynamics in the water column indicate a rapid response of the cyanobacterial community to these stratification and disturbance events, which were well-correlated with DO and P and metals stratification in the water column. We expect that internal P and trace metals dynamics are occurring over much shorter time-scales than could be measured by the current study design, and are more closely linked to the same external perturbations that were influencing the persistence of cyanobacterial blooms in Missisquoi Bay.

A conceptual model is presented to describe the seasonal evolution of P, Fe and Mn dynamics in shallow, eutrophic lake systems in the context of both internal and external drivers. In such systems, there is clearly a complex interplay between 'stable' and 'disturbed' water column states, which affects the distribution, concentration, and behavior of P, Fe and Mn in sediment and water column pools and exerts a strong effect on P-limited phytoplankton populations. We will discuss our understanding of these processes in relation to the following four major relevant themes: (1) the coupling between water column stability, P, and metals dynamics, (2) seasonal evolution of the sediment P and metals deficit, (3) sediment versus riverine sources of P and metals, (4) cyanobacterial persistence during the bloom season.

Coupling between water column stability, P, and metals dynamics

Water column P and metals dynamics responded rapidly to the development (or degradation) of water column stability in Missisquoi Bay. Water column stability, which is calculated based on thermal stratification [see eqs. (1) and (2)], was correlated with DO stratification throughout the bloom periods, particularly when wind speeds fell below the previously established mixing threshold of 4.5 m s^{-1} (Isles et al. 2015). Examples include the small, albeit significant, correlations between DO stratification and water column stability in the pre-bloom ($r = 0.1496$; $p < .0001$) and bloom collapse periods ($r = -0.2083$, $p < .0001$; Fig. 1), or the positive correlation found during the bloom period ($r = 0.5080$, $p < .0001$). Values of DO stratification in these correlations are based on YSI profiler data, which is systematically constrained to take measurements at a further distance from the SWI than can be achieved by manual sonde casts. In general, DO stratification was more pronounced in the manual data set (Fig. 2e) and, as confirmed by voltammetry (Fig. 5), illustrates the strong redox gradient that occurred within cm of the SWI and beyond the reach of the winch-sonde monitoring system.

Throughout the bloom season, calm periods lasting from days to weeks led to the establishment of a stable water column and DO stratification associated

with hypoxic or anoxic conditions at the SWI (Fig. 1c, d). In the absence of external disturbances, the development of reducing conditions at the SWI are primarily driven by the heterophic consumption of oxygen during the decay of organic matter in sediments, or a shift in the balance between algal photosynthesis and heterotrophic respiration, particularly in bottom waters where light penetration is limited (Coloso et al. 2011; Friedrich et al. 2014; Zilius et al. 2014). This was confirmed by Coloso et al. (2011), who found that short-term variations in water column stability (i.e., microstratification events) affected the distribution of algal cells throughout the water column, with consequences to the production of photosynthetically-derived dissolved oxygen at the surface and oxygen consumption in bottom waters. The majority of stratification events in the current study were associated with bottom water DO depletion (e.g., late in bloom onset, beginning and end of bloom period), though in some cases (e.g., JD 208 and later in bloom period, beginning late season bloom) 'microstratification' was due to DO enrichment in surface waters when BGA concentrations were also notably large (Fig. 1a, c, d). Wind-driven mixing as well as diminished water column stability and DO stratification occurred during multiple small events (<2 days) during the bloom period and during a more prolonged period of storm disturbance, which coincided with the beginning of the bloom collapse period (Fig. 1c, d).

In the absence of oxygen, the reductive dissolution of Mn- and Fe-oxide phases leads to the release of associated P from sediments, and the enrichment of sMn, sFe, and SRP concentrations in the bottom water (Hupfer and Lewandowski 2008; Smith et al. 2011). The coincidence between stable water column conditions, DO stratification, DO depletion, and sMn, sFe, and SRP enrichment in bottom waters was observed at discrete times within each of the identified bloom periods. Independent extract-based and voltammetric analyses (see below for more detail) show that solid phase redox sensitive Mn and Fe species were depleted with high dissolved concentrations reduced species in porewaters in the upper layer of sediments, which also corresponded to when sMn and sFe concentrations were elevated in bottomwater (Fig. 2b, c). In few cases, SRP was not enriched, but rather depleted in bottom water under these conditions (Fig. 2), which coincided with the borgeoning algal population (Fig. 1a) and high total P concentrations (Fig. 2d). This contrast in metal and SRP vertical concentration gradients was observed at the beginning of the pre-bloom, bloom onset, and late season bloom periods (Fig. 2). Collectively, these results suggest a close link between trace metal cycling, mobilization of sediment P, and the rapid consumption and partitioning of available P into developing cyanobacterial communities across the seasons.

Seasonal evolution of the sediment P, Fe, and Mn pools

We used an extract-based approach (i.e., ascrobate-citrate-bicarbonate) to assess the depletion or accumulation of reducible pools of P, Fe, and Mn in amorphous phase minerals. 'Reactive' P and metals reached maximum cumulative depletion (negative flux) prior to the start of the bloom period (JD 198) and the late season bloom (JD 260). The first major depletion of sediment P, Fe, and Mn on JD 198 was preceeded by a period of stable water column conditions and the enrichment of SRP, sMn, and sFe concentrations in the bottom waters indicative of reducing conditions at the SWI (as described above). In contrast, the second major depletion event occurred on JD 260 during the bloom collapse and following a large storm disturbance (Fig. 1f).

The large negative fluxes of reactive P and metals from the sediments in the bloom onset and bloom collapse periods were followed by the return of sediment reactive P and metals concentrations to near pre-bloom levels (Fig. 3) and slowing daily flux rates (Online Appendix 2). The sources and sinks of sediment P and metals are expected to vary over the course of the season based on algal bloom stage and other physical and abiotic characteristics of the system. For example, the re-accumulation of P and metals on JD 225 of the bloom period was preceded by a series of small storm events (Fig. 2d), diminished water column stability (Fig. 1c), and minimal depletion of bottom water DO (Fig. 1d). Soluble Fe and Mn concentrations near the SWI were low and daily sediment flux rates slowed in the bloom period, relative to bloom onset and the beginning of the bloom period. Bottom water SRP concentrations represented a small proportion of the estimated P loss from sediments during this period when BGA concentrations were largest. Sediment P accumulation in the first half of the bloom period, and the stabilization

of sediment concentrations in the second half, were related to wind- and discharge-driven disturbance and the oxygenation of surface sediments as indicated by increased DO concentrations in bottom waters. These conditions appear to have suppressed the sediment redox front, while riverine inputs of suspended sediment during small storm events could have negated any on-going redox-driven losses of P and Fe from sediments.

The storm event on JD 260 led to an influx of SRP and sFe concentrations and initiated a period of accumulation that would ultimately return the concentrations of sediment P and metals in the upper cm to within 22 % of pre-bloom conditions (Fig. 3a; Online Appendix 2). The timing and persistence of P, Fe, and Mn stabilization in sediments during this period indicate different source-sink dynamics and responses of P and metals to physical perturbation, which based on our hourly time-series can change dramatically over the course of hours. In addition to the wind-mixing event at the end of the bloom collapse period, decreasing water temperatures and declining BGA concentrations contribute to the diminishing biological productivity in the system. The release of available P and metals was observed in increasing concentrations of SRP, sMn, and sFe in the late bloom. However, the size of the soluble P and metals pools relative to their estimated accumulation in sediments varied. For example, daily sediment accumulation rates indicate 15–31 % of SRP and 41–66 % of sFe concentrations returned to sediments in the late season bloom. In contrast, Mn accumulation represented <1 to 8 % of the sMn measured above the SWI. This may indicate the slower return of Mn to the sediments or a substantial release of sMn from senescing cyanobacterial cells. It has been shown that cyanobacteria contain large cellular pools of phospholipid and polyphosphate P (Reitzel et al. 2012). Furthermore, cyanobacteria have a large demand for Mn as a cofactor for photosynthesis (Shcolnick and Keren 2006) and can accumulate up to two orders of magnitude more Mn than heterotrophic bacteria (Keren et al. 2002; Shcolnick and Keren 2006). The senescence of cyanobacteria blooms may therefore represent a significant return of both P and Mn to sediments at the end of a bloom season. Our group has found evidence for the deposition of P-containing organic detrital material during the collapse of previous blooms in Missisquoi Bay (Giles et al. 2015), however no previous reports have found an association of bloom die-off with cellular Mn deposition at the SWI. We speculate that external loading from the storm and an influx of organic material associated with the collapse of the summer bloom contributed to the composition and reaccumulation of Fe, Mn, and P in surface sediments.

During the relatively minor bloom conditions of this study, almost all of the P, Mn and Fe that were released from surface sediments during the pre-, onset and bloom periods had reaccumulated near the SWI by the autumn. This suggests that a relatively tight cycling of these constituents is occurring in shallow eutrophic systems, which may further explain the observed persistence of high aquatic P concentrations in catchments that have been subject to nutrient load regulation (Sharpley et al. 2013; Vandermolen and Boers 1994). Additionally, it has been established at this site (Schroth et al. 2015) that reducing conditions under ice can mobilize Fe, Mn, and P, enriching the upper sediment and potentially 'priming' the system with a more nutrient-enriched SWI for the next season. This work has important impications for the management of water quality in Missisquoi Bay and similar systems, particularly those which are hydrodynamically isolated and show little potential for the permanent removal of internal P loads. Specifically, our findings suggest that seasonal internal loading cycles of P will persist until the pool of labile P in the sediment is sufficiently depleted or ceases to be replenished. Additional detailed work examining the redox dynamics and speciation of Mn, Fe, and P at the SWI would provide a better understanding of exactly how the coupled deposition of watershed inputs and organic detritus could produce the trends observed here, which relied on operationally-defined metrics (i.e., selective extractions). The direct measurement of changes in the speciation and minerology of Fe, Mn, and P (e.g., XRD, XANES, EXAFS) upon controlled experimental manipulation of redox conditions at the SWI are a logical follow up to the time series data presented in our study.

Sediment versus riverine sources of P and metals

Our analysis indicates that elevated bottomwater sMn is a better indication of internal P loading than SRP or sFe concentrations. The reductive dissolution of Fe (oxy)hydroxide minerals in sediments results in the

solubilization of adsorbed P, which is immediately available for biological consumption and thus is not always detected as SRP in the water column time series. This reductive dissolution of Fe takes place lower in the sediment than Mn reduction (Fig. 5), with the Mn redox behavior indicating enhanced Fe-reduction closer to the surface. Due to the tight cycling of bioavailable phosphate that occurs in P limited systems, evidence of the mobilization of sediment P can be detected as increases in water column TP (as algal-P) or as an integrated signal of sediment P depletion over bimonthly to seasonal timescales. Manganese is more sensitive to reducing conditions than Fe and more stable in the dissolved phase. This supports the statistical analysis by Pearce et al. (2013), which suggested that elevated concentrations of Mn^{2+} could be used as a proxy for internal P loading to predict the onset of cyanobacterial blooms in Missisquoi Bay. Average summertime riverine soluble Mn concentrations of the Missisquoi River near its outlet are quite low (sMn 30 μg L^{-1}, n = 7), particularly during storm events, while soluble Fe and SRP tend to be relatively high (sFe 115 μg L^{-1}, SRP 28 μg L^{-1} n = 7; Schroth et al. 2015). Therefore, we interpret the signature of diminished sMn and elevated SRP and sFe in lake waters to indicate the influence of river inputs, particularly during periods of disturbance when the release of Mn from sediment redox processes is not possible.

The influence of influx of riverine suspended sediment on the composition of reactive P and metals in lake sediments was observed after the second major sediment depletion event on JD 260 (Fig. 3a). A decrease in the size of reactive-P and Fe pools typically represents the removal of these elements from the sediment via burial or internal loading processes; however, increases in the total AR-extractable concentrations during this storm period and large proportions of TP remaining in the water column suggests that the deposition of riverine suspended sediment may have introduced a pool of P to the sediment surface that was proportionally less labile/reducible (Online Appendix 2). Therefore, the depletion of reactive sediment P and metals pools is not limited to the calm, stratified conditions often associated with shifts in the sediment redox front, but may also reflect the introduction of riverine deposits or the redistribution of sediments with unique sediment compositions. Further work is needed to characterize suspended river sediments with regard to P retention capacity and trace metal composition and to assess the behavior of these constituents during the winter, particularly in the context of ice cover duration and the seasonal evolution of P and metals partitioning (Schroth et al. 2015).

Cyanobacterial persistence in the bloom season

Our analysis indicates that the 2013 algal bloom in Missisquoi Bay developed amidst P dynamics that were primarily controlled through the internal cycling of sediment P and inputs from riverine sources; however, the net removal of total and reducible forms of P and metals from sediments were limited by the end of the season. A prolonged period of warm, stable water column conditions initiated the bloom, which achieved relative maxima at multiple times during the study period due to the development of reducing conditions at the SWI and release of bioavailable P from Fe-oxide mineral phases. Prior to the start of the cyanobacterial bloom (pre-bloom and bloom onset), our data indicates the active release of P and trace metals from sediments, despite relatively depleted concentration of available P in surface and bottom waters. This suggests an alternative sink for bioavailable P in the water column, likely early season diatom blooms, which have been documented in this system previously (Isles et al. 2015). Upon intitiation of the cyanobacterial bloom, the dynamics of Fe, P and Mn were strongly influenced by the relative frequency and persistance of the lake being in a disturbed or calm state. The duration and degree of calm v. disturbed hydrodyamic states, coupled with the magnitude of riverine P, Fe, and Mn input, likely controls the rates of P accumulation and release as observed in the sediment and water column profiles, which will ultimately shape the intensity and timing of cyanobacterial blooms in shallow P-limited eutrophic systems.

In the autumn period, freshwater systems of the northeastern U.S. transition to lower average temperatures and become constently more well-mixed. As observed in Missisquoi Bay in 2013, this is characterized by the minimal stratification of DO, Mn, Fe or P and the accumulation of these constituents within the sediment profile. This is likely due to both riverine input of terrestrial sediment and reoxidation of reduced Fe to oxide phases that scavenge any

remaining soluble phosphate. Prolonged periods of unseasonably warm temperatures and low wind may lead to late season blooms, which respond quickly to short periods of relatively warm and more stable water column conditions. Transient stratification may also lead to P loading during this period due to the vertical advance of the redox front and associated reductive dissolution of Mn and Fe oxide phases near the SWI. Ultimately, as late autumn progresses, the system cools and becomes well-mixed due to disturbance, and little stratification and primary productivity is observed. In the sediment profile, reaccumulation of the reactive Fe, Mn, and P pools from the water column and biomass to the SWI occurs during this time frame. It should be noted that the bloom in 2013 was less intense than in previous years (Isles et al. 2015) and that additional studies will be needed to determine how P and trace metals cycling will vary in relatively strong bloom years.

Despite a significant release of bioavailable P into the water column during the late spring and summer, total and reducible forms of P were returned to the SWI by the autumn period. Historically, deforestation and the channelization of Vermont streams beginning in the 1800's led to a major redistribution of upland soils and has been detected in the paleolimnologic record near our study site (Burgess 2007; Marsden 1989). Diffuse and large-scale anthropogenic disturbaces still persist and may be directly influencing the biogeochemical conditions which exist today. For example, the construction of the VT route 78 causeway in 1938 largely separated Missisquoi Bay from the main body of Lake Champlain with the exception of a 200 m gap as the only point of surface water exchange (Marsden and Langdon 2012). The tight cycling of P in Missisquoi Bay reported in the current study and known physical constraints to the system suggest that P removal in this eutrophic system will be slow at best. This interpretation is based on measurements made at a single location in Missisquoi Bay and future studies should address the spatial variability of P and metals dynamics at the SWI (via sampling and modeling approaches) in order to identify sources and sinks of these mobile P pools. Due to the relative enrichment and stability of sediment labile P pools, succesful suppresion or reversal of the eutrophication of Missisquoi Bay and systems similar to it would likely hinge on mutli-pronged remediation strategies aimed at reduced P inputs from the watershed (e.g., agricultural best management practices, Sharpley et al. 2013) and the implementation of P recovery technologies (e.g., Elser and Bennett 2011).

Conclusions

We use a comprehensive monitoring approach to assess the internal and external drivers of P, Fe, and Mn dynamics at multiple time-scales during an algal bloom in a shallow, eutrophic system (Missisquoi Bay). Our study demonstrates the important role that water column stability and stratification play in the release of P and and trace metals from sediments and the establishment of harmful algal blooms. Importantly, stable hydrodynamic periods lasting from days to weeks influenced the extent of sediment P, Fe, and Mn flux, as well as the absolute and relative magnitude of soluble P, Fe, and Mn concentrations in bottom waters. We identify aqueous signatures of external riverine (i.e., SRP, sFe) and internal sediment inputs of P (i.e., SRP, sMn, sFe, DO depletion). Fluxes of P between the water column and the sediment were largely driven by the redox chemistry of Fe and Mn and DO depletion in bottom waters, which is biologically mediated by heterotrophic oxygen consumption and physically controlled by water column structure. Phosphorus bound to Fe-oxides and Mn-oxides appear to be tightly cycled over the course of the year, with the greatest release of P, Fe, and Mn from sediments occurring during the warmest and most hydrodynamically stable periods, and the greatest reaccumulation of reactive P, Fe, and Mn phases in sediments occuring during the late fall. We expect that hydrodynamic disturbances occuring on sub-daily time scales could trigger the release or reaccumulation of sediment P, Fe, and Mn over similar time scales. More frequent and direct measurements of redox species dynamics at the sediment water interface will be needed to confirm the timing of hydrodynamic-biogeochemical cascades that trigger or limit the development of harmful algal blooms. An understanding of the spatial distribution and frequency of hydrodynamically 'disturbed' or 'calm' states will be an integral component of predicting the biogeochemical response of similar aquatic systems to future climate change scenarios.

Acknowledgments We would like to thank the Research on Adaptation to Climate Change, Summer Internship Program

(2013–2014) interns and VT-EPSCoR support staff who contributed many hours directly and indirectly to this work. Thank you also to Andrea Lini and Gabriela Mora (University of Vermont, Geology) for their support in the sediment analysis component of this work. This research was supported by the Vermont Experimental Program to Stimulate Competitive Research with funds from the National Science Foundation Grant EPS-1101317 and a Biotechnology and Biological Sciences Research Council responsive mode grant (BBK0170471). Any opinions, findings, and conclusions or recommendations expressed in this material are those of the author(s) and do not necessarily reflect the views of the National Science Foundation.

References

Andersen FO, Ring P (1999) Comparison of phosphorus release from littoral and profundal sediments in a shallow, eutrophic lake. Hydrobiologia 408–409:175–183

Ann Y, Reddy KR, Delfino JJ (2000) Influence of redox potential on phosphorus solubility in chemically amended wetland organic soils. Ecol Eng 14(1–2):169–180

Anschutz P, Zhong SJ, Sundby B, Mucci A, Gobeil C (1998) Burial efficiency of phosphorus and the geochemistry of iron in continental margin sediments. Limnol Oceanogr 43(1):53–64. doi:10.4319/lo.1998.43.1.0053

Brendel PJ, Luther GW III (1995) Development of a gold amalgam voltammetric microelectrode for the determination of dissolved Fe, Mn, O2, and S(-II) in porewaters of marine and freshwater sediments. Environ Sci Technol 29(3):751–761. doi:10.1021/es00003a024

Buffle J, Zhand Z, Startchev K (2007) Metal flux and dynamic speciation at (Bio)interfaces. Part I: critical evaluation and compilation of physicochemical parameters for complexes with simple ligands and fulvic/humic acids. Environ Sci Technol 41(22):7609–7620. doi:10.1021/es070702p

Burgess H (2007) Geochemical indicators of productivity change in Lake Champlain, USA-Canada. M.S. Thesis. University of Vermont

Butterwick C, Heaney SI, Talling JF (2005) Diversity in the influence of temperature on the growth rates of freshwater algae, and its ecological relevance. Freshw Biol 50(2):291–300. doi:10.1111/j.1365-2427.2004.01317.x

Canfield DE et al (2005) The iron and manganese cycles. In: Kristensen E, Canfield DE, Bo T (eds) Advances in marine biology, Aquatic Geomicrobiology, vol 48. Elsevier Academic Press, London, pp 269–312

Coloso JJ, Cole JJ, Pace ML (2011) Short-term variation in thermal stratification complicates estimation of lake metabolism. Aquat Sci 73(2):305–315. doi:10.1007/s00027-010-0177-0

Cremona F, Laas A, Noges P, Noges T (2014) High-frequency data within a modeling framework: on the benefit of assessing uncertainties of lake metabolism. Ecol Model 294:27–35. doi:10.1016/j.ecolmodel.2014.09.013

Das SK, Routh J, Roychoudhury AN, Klump J, Ranjan RK (2009) Phosphorus dynamics in shallow eutrophic lakes: an example from Zeekoevlei, South Africa. Hydrobiologia 619:55–66. doi:10.1007/s10750-008-9600-0

Deborde J, Abrill G, Mouret A, Jezequel D, Thouzeau G, Clavier J, Bachelet G, Anschutz P (2008) Effects of seasonal dynamics in a Zostera noltii meadow on phosphorus and iron cycles in a tidal mudflat (Arcachon Bay, France). Mar Ecol Prog Ser 355:59–71. doi:10.3354/meps07254

Elser J, Bennett E (2011) Phosphorus cycle: a broken biogeochemical cycle. Nature 478(7367):29–31

Friedrich J, Janssen F, Aleynik D, Bange HW, Boltacheva N, Cagatay MN, Dale AW, Etiope G, Erdem Z, Geraga M, Gilli A, Gomoiu MT, Hall POJ, Hansson D, He Y, Holtappels M, Kirf MK, Kononets M, Konovalov S, Lichtschlag A, Livingstone DM, Marinaro G, Mazlumyan S, Naeher S, North RP, Papatheodorou G, Pfannkuche O, Prien R, Rehder G, Schubert CJ, Soltwedel T, Sommer S, Stahl H, Stanev EV, Teaca A, Tengberg A, Waldmann C, Wehrli B, Wenzhofer F (2014) Investigating hypoxia in aquatic environments: diverse approaches to addressing a complex phenomenon. Biogeosciences 11(4):1215–1259. doi:10.5194/bg-11-1215-2014

Froelich PN, Klinkhammer GP, Bender ML, Luedtke NA, Heath GR, Cullen D, Dauphin P, Hammond D, Hartman B, Maynard V (1979) Early oxidation of organic matter in pelagic sediments of the eastern equatorial Atlantic: suboxic diagenesis. Geochim Cosmochim Acta 43(7):1075–1090. doi:10.1016/0016-7037(79)90095-4

Giles CD, Lee LG, Cade-Menun BJ, Hill JE, Isles PDF, Schroth AW, Druschel GK (2015) Characterization of organic phosphorus form and bioavailability in lake sediments using ^{31}P nuclear magnetic resonance and enzymatic hydrolysis. J Environ Qual 44:882–894. doi:10.2134/jeq2014.06.0273

Hegmen W, Wang D, Borer C (1999) Estimation of Lake Champlain basinwide nonpoint source. In: Technical report number 31. Lake Champlain Basin Program

Holdren GC, Armstrong DE (1980) Factors affecting phosphorus release from intact lake sediment cores. Environ Sci Technol 14(1):79–87. doi:10.1021/es60161a014

Huber V, Wagner C, Gerten D, Adrian R (2012) To bloom or not to bloom: contrasting responses of cyanobacteria to recent heat waves explained by critical thresholds of abiotic drivers. Oecologia 169(1):245–256. doi:10.1007/s00442-011-2186-7

Huisman J, Sharples J, Stroom JM, Visser PM, Kardinaal WEA, Verspagen JMH, Sommeijer B (2004) Changes in turbulent mixing shift competition for light between phytoplankton species. Ecology 85(11):2960–2970. doi:10.1890/03-0763

Hupfer M, Lewandowski J (2008) Oxygen controls the phosphorus release from lake sediments—a long-lasting paradigm in limnology. Int Rev Hydrobiol 93(4–5):415–432. doi:10.1002/iroh.200711054

Isles PDF, Giles CD, Gearhart TA, Xu Y, Druschel GK, Schroth AW (2015) Dynamic internal drivers of a historically severe cyanobacteria bloom in Lake Champlain revealed through comprehensive monitoring. J Great Lakes Res 41(3):818–829. doi:10.1016/j.jglr.2015.06.006

Katsev S, Dittrich M (2013) Modeling of decadal scale phosphorus retention in lake sediment under varying redox conditions. Ecol Model 251:246–259. doi:10.1016/j.ecolmodel.2012.12.008

Keren N, Kidd MJ, Penner-Hahn JE, Pakrasi HB (2002) A light-dependent mechanism for massive accumulation of

manganese in the photosynthetic bacterium *Synechocystis* sp. PCC 6803. Biochemistry 41(50):15085–15092

Konopka A, Brock TD (1978) Effect of temperature on blue-green algae (cyanobacteria) in Lake Mendota. Appl Environ Microbiol 36(4):572–576

Lurling M, Eshetu F, Faassen EJ, Kosten S, Huszar VLM (2013) Comparison of cyanobacterial and green algal growth rates at different temperatures. Freshw Biol 58(3):552–559. doi:10.1111/j.1365-2427.2012.02866.x

Madison AS, Tebo BM, Mucci A, Sundby B, Luther GW (2013) Abundant porewater Mn(III) is a major component of the sedimentary redox system. Science 341(6148):875–878. doi:10.1126/science.1241396

Marsden MW (1989) Lake restoration by reducing external phosphorus loading—the influence of sediment phosphorus release. Freshw Biol 21(2):139–162. doi:10.1111/j.1365-2427.1989.tb01355.x

Marsden JE, Langdon RW (2012) The history and future of Lake Champlain's fishes and fisheries. J Great Lakes Res 38(Supplement 1):19–34. doi:10.1016/j.jglr.2011.09.007

Moore PA, Reddy KR, Fisher MM (1998) Phosphorus flux between sediment and overlying water in Lake Okeechobee, Florida: spatial and temporal variations. J Environ Qual 27(6):1428–1439

Olila OG, Reddy KR (1997) Influence of redox potential on phosphate-uptake by sediments in two sub-tropical eutrophic lakes. Hydrobiologia 345:45–57. doi:10.1023/a:1002975231341

O'Neil JM, Davis TW, Burford MA, Gobler CJ (2012) The rise of harmful cyanobacteria blooms: the potential roles of eutrophication and climate change. Harmful Algae 14:313–334. doi:10.1016/j.hal.2011.10.027

Pearce AR, Rizzo DM, Watzin MC, Druschel GK (2013) Unraveling associations between cyanobacteria blooms and in-lake environmental conditions in Missisquoi Bay, Lake Champlain, USA, using a modified self-organizing map. Environ Sci Technol 47(24):14267–14274. doi:10.1021/es403490g

Reitzel K, Ahlgren J, Rydin E, Egemose S, Turner BL, Hupfer M (2012) Diagenesis of settling seston: identity and transformations of organic phosphorus. J Environ Qual 14(3):1098–1106. doi:10.1039/c2em10883f

Reynolds CS, Oliver RL, Walsby AE (1987) Cyanobacterial dominance: the role of buoyancy regulation in dynamic lake environments. NZ J Mar Freshwat Res 21(3):379–390. doi:10.1080/00288330.1987.9516234

Schroth AW, Giles CD, Isles PDF, Xu Y, Perzan Z, Druschel GK (2015) Dynamic coupling of iron, manganese, and phosphorus behavior in water and sediment of shallow ice-covered eutrophic lakes. Environ Sci Technol 49(16):9758–9767. doi:10.1021/acs.est.5b02057

Sharpley A, Jarvie HP, Buda A, May L, Spears B, Kleinman P (2013) Phosphorus Legacy: overcoming the effects of past management practices to mitigate future water quality impairment. J Environ Qual 42(5):1308–1326. doi:10.2134/jeq2013.03.0098

Shcolnick S, Keren N (2006) Metal homeostasis in cyanobacteria and chloroplasts. Balancing benefits and risks to the photosynthetic apparatus. Plant Physiol 141(3):805–810. doi:10.1104/pp.106.079251

Shiller AM (2003) Syringe filtration methods for examining dissolved and colloidal trace element distributions in remote field locations. Environ Sci Technol 37(17):3953–3957. doi:10.1021/es0341182

Slowey A, Marvin-DiPasquale M (2012) How to overcome inter-electrode variability and instability to quantify dissolved oxygen, Fe(II), mn(II), and S(II) in undisturbed soils and sediments using voltammetry. Geochem Trans 13(1):6

Smith L, Watzin MC, Druschel G (2011) Relating sediment phosphorus mobility to seasonal and diel redox fluctuations at the sediment-water interface in a eutrophic freshwater lake. Limnol Oceanogr 56(6):2251–2264. doi:10.4319/lo.2011.56.6.2251

Sondergaard M, Jeppesen E, Lauridsen TL, Skov C, Van Nes EH, Roijackers R, Lammens E, Portielje R (2007) Lake restoration: successes, failures and long-term effects. J Appl Ecol 44(6):1095–1105. doi:10.1111/j.1365-2664.2007.01363.x

Thomas DB, Schallenberg M (2008) Benthic shear stress gradient defines three mutually exclusive modes of non-biological internal nutrient loading in shallow lakes. Hydrobiologia 610:1–11. doi:10.1007/s10750-008-9417-x

Torremorell A, Llames ME, Perez GL, Escaray R, Bustingorry J, Zagarese H (2009) Annual patterns of phytoplankton density and primary production in a large, shallow lake: the central role of light. Freshw Biol 54(3):437–449. doi:10.1111/j.1365-2427.2008.02119.x

Troy A, Wang D, Capen D, O'Neil Dunne J, MacFaden S (2007) Updating the Lake Champlain basin land use data to improve prediction of phosphorus loading. In: Technical Report 54. Lake Champlain Basin Program

USEPA (1996) Test Method 3050B: Acid digestion of sediments, sludges, soils. In: SW-846, test methods for evaluating solid waste: Physical/chemical methods. SW-846. United States Environmental Protection Agency

Vandermolen DT, Boers PCM (1994) Influence of internal loading on phosphorus concentration in shallow lakes before and after reduction of the external loading. Hydrobiologia 275:379–389. doi:10.1007/BF00026728

VTDEC (2008) Vermont Department of Environmental Conservation. Lake Champlain long-term monitoring program. http://www.watershedmanagement.vt.gov/lakes/htm/lp_longterm.htm. Accessed 23 Nov 2015

Xu Y, Schroth AW, Rizzo DM (2015) Developing a 21st century framework for lake-specific eutrophication assessment using quantile regression. Limnol Oceanogr Methods 13(5):237–249. doi:10.1002/lom3.10021

Zamyadi A, McQuaid N, Prevost M, Dorner S (2012) Monitoring of potentially toxic cyanobacteria using an online multi-probe in drinking water sources. J Environ Monit 14(2):579–588. doi:10.1039/c1em10819k

Zilius M, Bartoli M, Bresciani M, Katarzyte M, Ruginis T, Petkuviene J, Lubiene I, Giardino C, Bukaveckas PA, de Wit R, Razinkovas-Baziukas A (2014) Feedback mechanisms between cyanobacterial blooms, transient hypoxia, and benthic phosphorus regeneration in shallow coastal environments. Estuaries Coasts 37(3):680–694. doi:10.1007/s12237-013-9717-x